Mass Function of Binary Massive Black Holes in Active Galactic Nuclei

Kimitake Hayasaki

Department of Physics, Graduate School of Science, Hokkaido University Kitaku, Sapporo 060-0810, Japan

hayasakin@astro1.sci.hokudai.ac.jp

Yoshihiro Ueda

Department Astronomy, Kyoto University Oiwake-cho, Kitashirakawa, Sakyo-ku, Kyoto 606-8502

Naoki Isobe

Department Astronomy, Kyoto University Oiwake-cho, Kitashirakawa, Sakyo-ku, Kyoto 606-8502

(Received 2010 January 18; accepted)

Abstract

If the activity of active galactic nuclei (AGNs) is predominantly induced by major galaxy mergers, then a significant fraction of AGNs should harbor binary massive black holes in their centers. We study the mass function of binary massive black holes in nearby AGNs based on the observed AGN black-hole mass function and theory of evolution of binary massive black holes interacting with a massive circumbinary disk in the framework of coevolution of massive black holes and their host galaxies. The circumbinary disk is assumed to be steady, axisymmetric, geometrically thin, self-regulated, self-gravitating but non-fragmenting with a fraction of Eddington accretion rate, which is typically one tenth of Eddington value. The timescale of orbital decay is then estimated as $\sim 10^8$yr for equal mass black-hole, being independent of the black hole mass, semi-major axis, and viscosity parameter but dependent on the black-hole mass ratio, Eddington ratio, and mass-to-energy conversion efficiency. This makes it possible for any binary massive black holes to merge within a Hubble time by the binary-disk interaction. We find that $(1.8 \pm 0.6\%)$ for the equal mass ratio and $(1.6 \pm 0.4\%)$ for the one-tenth mass ratio of the total number of nearby AGNs have close binary massive black holes with orbital period less than ten years in their centers, detectable with on-going highly sensitive X-ray monitors such as *Monitor of All-sky X-ray Image* and/or *Swift*/Burst Alert Telescope. Assuming that all binary massive black holes have the equal mass ratio, about 20% of AGNs with black hole masses of $10^{6.5-7} M_\odot$ has the close binaries and thus provides the best chance to detect them.

Key words: black hole physics – accretion, accretion disks – binaries:general – galaxies:nuclei

1. Introduction

Most galaxies are thought to have massive black holes at their centers (Kormendy & Richstone 1995). Massive black holes play an important role not only in the activities of active galactic nuclei (AGNs) and quasars but also in the formation and evolution of galaxies(Magorrian et al. 1998; Ferrarese&Merritt 2000; Gebhardt et al. 2000). Galaxy merger leads to the mass inflow to the central region by tidal interactions and then a nucleus of the merged galaxy is activated and black hole grows by gas accretion (Yu & Tremaine 2002). At some step, the outflow from the central black hole sweeps away the surrounding gas and quenches the star formation and black hole growth. This also produces an observed correlation between the black hole mass and velocity dispersion of individual galaxies (Di Matteo et al. 2005).

During a sequence of processes, binary massive black holes with a subparsec-scale separation are inevitably formed before two black holes merge by emitting gravitational radiation. Recent hydrodynamic simulations showed the rapid binary black hole formation in the parsec scale within several Gyrs by the interaction between the black holes and the surrounding stars and gas in gas-rich galaxy merger (Dotti et al. 2007; Mayer et al. 2007). Even if there are transiently triple massive black holes in a galactic nucleus, the system finally settles down to the formation of binary massive black holes by merging of two black hole or by ejecting one black hole from the system via a gravitational slingshot (Iwasawa et al. 2006).

In coalescing process of two massive black hole, there has been the so-called final parsec problem: it is still unknown how binary massive black holes evolve after its semi-major axis reached to the subparsec scale where the dynamical friction with the neighboring stars is no longer effective. Many authors have tackled the final parsec problem in the context of the interaction between the black holes and the stars, but there has been still extensive discussions (Begelman et al. 1980; Makino 1997; Quinlan & Hernquist 1997; Milosavljević & Merritt 2003; Sesana et al. 2007; Matsubayashi et al. 2007; Matsui & Habe 2009). There is other possible way to extract the energy and the angular momentum from binary massive black holes by the interaction between the black holes and the gas surrounding them. This kind of the binary-disk interaction could also be the candidate to resolve the final parsec problem (Ivanov et al. 1999; Gould & Rix 2000; Armitage & Natarajan 2002; Armitage & Natarajan 2005; Escala et al. 2005; Hayasaki 2009; Cuadra et al. 2009; Haiman et al. 2009) in spite of a claim(Lodato et al. 2009). Some authors showed that there exist close binary massive black holes with a short orbital period less than ten years and significant orbital eccentricity(Armitage & Natarajan 2005; Hayasaki 2009; Cuadra et al. 2009).

Hayasaki et al. (2007) studied the accretion flow from a circumbinary disk onto binary massive black holes, using a smoothed particle hydrodynamics (SPH) code. They found that mass transfer occurs from the circumbinary disk to each black hole. The mass accretion rate significantly depends on the binary orbital phase in eccentric binaries, whereas it shows little

variation with orbital phase in circular binaries. Periodic behaviors of the mass accretion rate in the binary system with the different geometries or system parameters were also discussed by some other authors(Bogdanović et al. 2008; MacFadyen & Milosavljević 2008; Cuadra et al. 2009). Recently, Bogdanović et al. (2009) and Dotti et al. (2009) proposed the hypothesis that SDSSJO92712.65+294344.0 consists of two massive black holes in binary, by interpreting the observed emission line features as those arising from the mass-transfer stream from the circumbinary disk.

Hayasaki et al. (2008) have, furthermore, performed a new set of simulations at higher resolution with an energy equation based on the blackbody assumption, adopting the same set of binary orbital parameters we had previously used (Hayasaki et al. 2007) ($a = 0.01\,\mathrm{pc}$, eccentricity $e = 0.5$, and mass ratio $q = 1.0$). By this two-stage simulation, they found that while the Optical/NIR light curve exhibits little variation, the X-ray/UV light curve shows significant orbital modulation in the triple-disk system, which consists of an accretion disk around each black hole and a circumbinary disk around them. X-ray/UV periodic light variation are originated from a phase-dependent mass transfer from circumbinary disk (cf. Hayasaki & Okazaki 2005). The one-armed spiral wave on the accretion disk induced by the phase-dependent mass transfer causes the mass to accrete onto each black hole within one orbital period. This is repeated every binary orbit. These unique light curves are, therefore, expected to be one of observational signatures of binary massive black holes.

Highly sensitive X-ray monitors over a wide area provide us with a unique opportunity to discover close binary massive black holes in an unbiased manner, based on the detection of the orbital flux modulation. Monitor of All-sky X-ray Image (MAXI; Matsuoka et al. 2009), a Japanese experimental module attached to the International Space Station, is now successful in operation since the launch in 2009 July. MAXI, covering the energy band of 0.5–30 keV, achieves a significantly improved sensitivity as an all X-ray monitor compared with previous missions. According to the hard X-ray luminosity function of AGNs by Ueda et al. (2003), $\approx$1,300 nearby AGNs can be detected at the confusion flux limit of $\sim$0.2 mCrab from the extragalactic sky at galactic latitudes higher than 10°. Among them, the brightest $\sim$100 AGNs can be monitored every 2 months with a flux accuracy of 20% level. Over the plausible mission life of MAXI ($\geq 2\,\mathrm{yr}$), it is possible to detect binary massive black holes in nearby AGNs with binary orbital periods less than 10 yr. Besides MAXI, the Swift/Burst Alert Telescope (BAT) survey (Tueller et al. 2010) can make a similar job in the hard X-ray band of 15–200 keV.

In this paper, we investigate mass functions of binary massive black holes with a very-short orbital period detectable with MAXI and/or Swift/BAT. The plan of this paper is organized as follows. In Section 2, we describe the evolutionary scenario of binary massive black holes in the framework of coevolution of massive black holes and their host galaxies. Section 3 shows mass functions of close binary massive black holes. They can be written as the product of the observed black-hole mass function of nearby AGNs and probability for finding binary mas-

sive black holes, based on the evolutionary scenario as described in Section 2. Brief discussions and conclusions are summarized in Section 4.

2. Final-parsec evolution of binary massive black holes

We first describe the evolution of binary massive black holes, focusing on interaction with surrounding gaseous disks in the framework of coevolution of massive black holes and their host galaxies.

Does the black hole mass correlate with the velocity dispersion of bulge in individual galaxies despite that there is a single or binary in their center? This is one of fundamental problems in the framework of the coevolution of massive black holes and their host galaxies. In some elliptical galaxies, there is a core with the outer steep brightness and inner shallow brightness. Binary massive black holes are considered to be closely associated with such a core structure with the mass of stellar light deficit(Ebisuzaki et al. 1991; Milosavljević & Merritt 2001). Recently, Kormendy & Bender (2009) showed the tight correlations among black hole masses, velocity dispersions of host galaxies, and masses of stellar light deficits, using the observational data of 11 elliptical galaxies with cores. This suggests that these correlations are still held for even if there are not only a single massive black hole but also binary massive black holes in cores of elliptical galaxies.

Binary massive black holes are considered mainly to evolve via three stages (Begelman et al. 1980). Firstly, each of black holes sinks independently towards the center of the common gravitational potential due to the dynamical friction with neighboring stars. If the binary can be regarded as a single black hole, its gravitational influence radius to the field stars is defined as

$$r_{\rm inf} = \frac{GM_{\rm bh}}{\sigma_*^2} \sim 3.4[{\rm pc}] \left(\frac{\rm M_{bh}}{10^7 {\rm M}_\odot} \right)^{1-2/\beta_2}, \tag{1}$$

where the tight correlation between the black hole mass and one-dimensional velocity dispersion, σ_*, of the stars, the so-called $M_{\rm bh} - \sigma_*$ relation: $M_{\rm bh}/10^7 M_\odot = \beta_1 \left(\sigma_*/200{\rm kms}^{-1}\right)^{\beta_2}$ is made use of. Unless otherwise noted, $\beta_1 = 16.6$ and $\beta_2 = 4.86$ are adopted by (Merritt & Milosavljević 2005) in what follows.

When the separation between two black holes becomes less than 1 pc or so, angular momentum loss by the dynamical friction slows down due to the loss-cone effect and a massive hard binary is formed. This is the second stage. The binary harden at the radius where the kinetic energy per unit mass of the star with σ_*, equals to the binding energy per unit mass of the binary(Quinlan 1996). Its hardening radius is defined as

$$a_{\rm h} = \frac{1}{4} \frac{q}{(1+q)^2} r_{\rm inf} \sim 8.5 \times 10^{-1} [{\rm pc}] \frac{\rm q}{(1+{\rm q})^2} \left(\frac{\rm M_{bh}}{10^7 {\rm M}_\odot} \right)^{1-2/\beta_2}, \tag{2}$$

where q is the black-hole mass ratio.

Finally, the semi-major axis of the binary decreases the radius at which the gravitational radiation dominates, and then a pair of black holes merge into a single supermassive black hole. The detailed timescale in each evolutionary phase will be described in the following three subsections.

2.1. Star driven phase

2.1.1. The dynamical friction

Each black hole sinks into the common center of mass due to the dynamical friction with ambient field stars. The merger rate of two black holes is given by(Binney & Tremaine 1987)

$$\frac{\dot{a}(t)}{a(t)} = -\frac{0.428}{\sqrt{2}} \ln\Lambda \frac{GM_{\rm bh}}{\sigma_*} \frac{1}{a^2(t)}, \tag{3}$$

where $a(t)$ is the separation between two black holes and $\ln\Lambda \approx 10$ is the Coulomb logarithm. The decaying timescale of black-hole orbits is then written

$$t_{\rm df} = \left|\frac{a(t)}{\dot{a}(t)}\right| \sim 8.4\times10^6[{\rm yr}] \left(\frac{\rm a(t)}{\rm a_0}\right)^2 \left(\frac{\rm M_{bh}}{10^7 M_\odot}\right)^{1/\beta_2-1}, \tag{4}$$

where $a_0 = 100$pc is the typical core radius of the host galaxy. The integration of merger rate gives the following equation

$$\frac{a(t)}{a_0} = \left(1 - \frac{t}{t_{\rm c}^{\rm df}}\right)^{1/2}, \tag{5}$$

where

$$t_{\rm c}^{\rm df} \sim 4.2\times10^6[{\rm yr}] \left(\frac{\rm a_0}{100{\rm pc}}\right)^2 \left(\frac{\rm M_{bh}}{10^7 M_\odot}\right)^{1/\beta_2-1}. \tag{6}$$

Recall that $\beta_2 \sim 5$, and hence the index of mass dependence is $-4/5$ for both $t_{\rm df}$ and $t_{\rm c}^{\rm df}$.

2.1.2. Stellar scattering

Even after hardening of the binary, the binary orbit continues to decay by loss cone refilling of stars due to the two-body relaxation. In addition, the repeated gravitational slingshot interactions with stars makes the orbital decay significantly rapid for black hole with mass less than few$\times10^6 M_\odot$. For the system with a singular isothermal sphere, the timescale is given as(Milosavljević & Merritt 2003)

$$t_{\rm ss} = \left|\frac{a(t)}{\dot{a}(t)}\right| \sim 3.0\times10^8[{\rm yr}] \left(\frac{a_{\rm h}}{a(t)}\right) \left(\frac{M_{\rm bh}}{10^7 M_\odot}\right). \tag{7}$$

For the black hole with mass greater than $10^{6.5} M_\odot$, this mechanism contributes inefficiently to the orbital decay of the binary on the subparsec scale. Instead, the binary-disk interaction is likely to be a dominant mechanism of the orbital decay. Quite recent N-body simulations show that stellar dynamics alone can also resolve the final parsec problem (e.g., Berentzen et al. 2009).

2.2. Gaseous-disk driven phase

The circumbinary disk would be formed inside the gravitational influence radius after hardening of the binary. The inner edge of circumbinary disk is then defined as

$$r_{\rm in} = \left(\frac{m+1}{l}\right)^{2/3} a(t)$$
$$\sim 1.8[{\rm pc}]\frac{q}{(1+q)^2}\left(\frac{M_{\rm bh}}{10^7 M_\odot}\right)^{1-2/\beta_2}\left(\frac{a(t)}{a_{\rm h}}\right), \quad (8)$$

where $a(t)$ is the semi-major axis of binary, and $m=2$ and $l=1$ are adopted unless otherwise noted(Artymowicz & Lubow 1994).

For simplicity, the circumbinary disk is assumed to be a steady, axisymmetric, and geometrically thin with a differential rotation and fraction of Eddington accretion rate:

$$\dot{M}_{\rm acc} = \eta \dot{M}_{\rm Edd}$$
$$\sim 2.2\times 10^{-2}\left[\frac{M_\odot}{\rm yr}\right]\left(\frac{\eta}{0.1}\right)\left(\frac{0.1}{\epsilon}\right)\left(\frac{M_{\rm bh}}{10^7 M_\odot}\right), \quad (9)$$

where η, ϵ and $\dot{M}_{\rm Edd}$ are the Eddington ratio, mass-to-energy conversion efficiency, and Eddington accretion rate defined by $\dot{M}_{\rm Edd} = (1/\epsilon)4\pi G M_{\rm bh} m_{\rm p}/c\sigma_{\rm T}$, where $m_{\rm p}$, c, and $\sigma_{\rm T}$ show the proton mass, light velocity, and Thomson scattering cross section, respectively.

The surface density of circumbinary disk can be then written as

$$\Sigma = \frac{\dot{M}_{\rm acc}}{2\pi\nu}\left|\frac{d\ln r}{d\ln\Omega}\right|. \quad (10)$$

where the eddy viscosity is defined as $\nu = \alpha c_{\rm cv} H$ with the Shakura-Sunyaev viscosity parameter(Shakura & Sunyaev 1973), α, characteristic velocity, $c_{\rm cv}$, and disk scale-hight, H.

The stability criterion for self-gravitation of the disk is defined by the Toomre Q-value: $Q = \Omega c_{\rm cv}/\pi G\Sigma$. If the disk structure obeys a *standard disk* with $\dot{M}_{\rm acc}$ with $\eta = 0.1$, Q is much less than 1. This means that the disk is massive enough to be gravitationally unstable. Therefore, we introduce a self-regulated, self-gravitating disk model (Mineshige & Umemura 1996; Bertin 1997). The condition of self-regulated disk is given by

$$Q \approx 1. \quad (11)$$

From equations (10) and (11), the effective sound velocity of self-gravitating disk is written as

$$c_{\rm sg} = \left[\frac{G\dot{M}_{\rm acc}}{2\alpha_{\rm sg}}\left|\frac{\ln r}{\ln\Omega}\right|\right]^{1/3}, \quad (12)$$

where we adopt $\alpha = \alpha_{\rm sg} \lesssim 0.06$ and $c_{\rm cv} = c_{\rm sg}$. If the radiative cooling in the disk is so efficient, the disk would fragment. The criterion whether the disk fragment or not is given by $\alpha_{\rm sg} = 0.06$(Rice et al. 2005). If $\alpha_{\rm sg} > 0.06$, the fragmentation occurs in the disk and causes the subsequent star formation. Such a situation is beyond the scope of our disk model. Assuming that the disk face radiates as a blackbody, the sound velocity can be written

$$c_{\rm s} = \left(\frac{R_{\rm g}}{\mu}\right)^{1/2} \left(\frac{3GM_{\rm bh}\dot{M}_{\rm acc}}{8\pi r^3\sigma}\right)^{1/8}, \tag{13}$$

where $R_{\rm g}$, μ, and σ are the gas constant, molecular weight, and Stefan-Bolzmann constant, respectively.

The self-gravity of the disk is stronger than the gravity of the central black hole at the self-gravitating radius where the total disk mass equals to the black hole mass. The rotation velocity of the disk then become flat outside the self-gravitating radius:

$$\begin{aligned} r_{\rm sg} &\approx \frac{GM_{\rm bh}}{8}\left(\frac{G\dot{M}_{\rm acc}}{2\alpha_{\rm sg}}\right)^{-2/3} \\ &\sim 64[{\rm pc}]\left(\frac{\alpha_{\rm sg}}{0.06}\right)^{2/3}\left(\frac{0.1}{\epsilon}\right)^{-2/3}\left(\frac{\eta}{0.1}\right)^{-2/3}\left(\frac{\rm M_{bh}}{10^7{\rm M}_\odot}\right)^{1/3}, \end{aligned} \tag{14}$$

where we put $c_{\rm cv} = c_{\rm sg}$. Inside $r_{\rm sg}$, the angular frequency of the disk corresponds to Keplerian one where the gravity of central black hole dominates the dynamics of the disk. When $c_{\rm cv} = c_{\rm s}$, the disk transits from the self-regulated, self-gravitating disk to standard disk. Its radius is given as

$$\begin{aligned} r_{\rm stsg} &= \left(\frac{R_{\rm g}}{\mu}\right)^{4/3}\left(\frac{G\dot{M}_{\rm acc}}{2\alpha_{\rm sg}}\right)^{-8/9}\left(\frac{3GM_{\rm bh}\dot{M}_{\rm acc}}{8\pi\sigma}\right)^{1/3} \\ &\sim 4.4\times10^{-4}[{\rm pc}]\left(\frac{\alpha_{\rm sg}}{0.06}\right)^{8/9}\left(\frac{0.1}{\epsilon}\right)\left(\frac{\eta}{0.1}\right)\left(\frac{\rm M_{bh}}{10^7{\rm M}_\odot}\right)^{-2/9}. \end{aligned} \tag{15}$$

As the binary evolves, the disk structure gets to depend on black hole mass. Since $r_{\rm in}(a_{\rm h})$ is less than $r_{\rm sg}$ and more than $r_{\rm stsg}$ in the all black-hole mass range, the circumbinary disk is initially modeled as the self-regulated, self-gravitating disk with the Keplerian rotation. When the semi-major axis decays to the decoupling radius defined by equations (25) and (26), $r_{\rm in}(a_{\rm d})$ is less than $r_{\rm stsg}$ for $10^5 M_\odot \le M_{\rm bh} \lesssim 3\times10^6 M_\odot$. The disk structure for $10^5 \le M_{\rm bh} \lesssim 3\times10^6 M_\odot$ can then be described by the standard disk theory, whereas the disk still remains to be the self-regulated, self-gravitating disk with Keplerian rotation for other black-hole mass ranges (see the dotted line of Fig. 2).

The circumbinary disk and binary exchanges the energy and angular momentum through the tidal/resonant interaction. For moderate orbital-eccentricity range, the torque of binary potential dominantly acts on the circumbinary disk at the 1:3 outer Lindblad resonance radius where the binary torque is balanced with the viscous torque(Artymowicz & Lubow 1994).

On the other hand, the circumbinary disk deforms to be elliptical by the tidal/resonant interaction. The density of gas is locally enhanced by the gravitational potential at the closest two points from each black hole on the inner edge of circumbinary disk (Hayasaki et al. 2007). The angular momentum of gas is removal by the locally enhanced viscosity, and thus the gas overflows from the two points to the central binary. An accretion disk is then formed around each black hole by the transferred gas(Hayasaki et al. 2008). The mass transfer therefore adds

its angular momentum to the binary via two accretion disks(Hayasaki 2009).

In a steady state, the mass transfer rate equals to the accretion rate, $\dot{M}_{\rm acc}$. Since it is much smaller than the critical transfer rate defined by equation (41) of Hayasaki (2009), the effect of torque by the mass transfer torque can be neglected. The orbital-decay rate is then approximately written by equation (40) of Hayasaki (2009) as

$$\frac{\dot{a}(t)}{a(t)} \approx -\frac{\dot{J}_{\rm cbd}}{J_{\rm b}}\sqrt{1-e^2}, \tag{16}$$

where e is the orbital eccentricity of the binary and the net torque, $\dot{J}_{\rm cbd}$, from the binary to circumbinary disk can be approximately written as

$$\dot{J}_{\rm cbd} \approx 3^{4/3}\frac{(1+q)^2}{q}\frac{1}{t_{\rm vis,in}}\frac{M_{\rm ld}}{M_{\rm bh}}\frac{J_{\rm b}}{\sqrt{1-e^2}}, \tag{17}$$

where $t_{\rm vis,in}=r_{\rm in}^2/\nu_{\rm in}=\sqrt{GM_{\rm bh}r_{\rm in}}/(\alpha c_{\rm cv}^2)$ is the viscous timescale measured at the inner edge of disk and $M_{\rm ld}$ is the local disk mass defined as $M_{\rm ld}=\pi r_{\rm in}^2\Sigma_{\rm in}$. From equation (10), the product of the viscous timescale and ratio of the black hole mass to local disk mass is given by

$$t_{\rm vis,in}\left(\frac{M_{\rm ld}}{M_{\rm bh}}\right)^{-1} = 2\frac{M_{\rm bh}}{\dot{M}_{\rm acc}}\left|\frac{d\ln\Omega}{d\ln r}\right|. \tag{18}$$

Substituting equation (17) with equation (18) into equation (16), the orbital-decay rate can be expressed by

$$\frac{\dot{a}(t)}{a(t)} = -\frac{1}{t_{\rm c}^{\rm gas}}, \tag{19}$$

where $t_{\rm c}^{\rm gas}$ is the characteristic timescale of orbital decay due to the binary-disk interaction:

$$\begin{aligned} t_{\rm c}^{\rm gas} &= \frac{2}{3^{4/3}}\frac{q}{(1+q)^2}\frac{M_{\rm bh}}{\dot{M}_{\rm acc}}\left|\frac{d\ln\Omega}{d\ln r}\right| \\ &\sim 3.1\times10^8[{\rm yr}]\frac{\rm q}{(1+{\rm q})^2}\left(\frac{0.1}{\eta}\right)\left(\frac{\epsilon}{0.1}\right), \end{aligned} \tag{20}$$

where we adopt $\Omega=\Omega_{\rm K}$. Note that $t_{\rm c}^{\rm gas}$ is independent of the black-hole mass, semi-major axis, and viscosity parameter, but dependent on the black-hole mass ratio, Eddington ratio, and mass-to-energy conversion efficiency. These arise from the assumptions that the disk is axisymmetric with a fraction of Eddington accretion rate and its angular momentum is outwardly transferred by the viscosity of Shakura-Sunyaev type.

Integrating equation (19), we obtain

$$\frac{a(t)}{a_{\rm h}} = \exp\left(-\frac{t}{t_{\rm c}^{\rm gas}}\right). \tag{21}$$

Following equations (29) of Hayasaki (2009), the orbital eccentricity increases with time in the present disk model. The orbital eccentricity is, however, expected to saturate during the disk-driven phase, because the angular momentum of the binary is mainly transferred to the circumbinary disk when the binary is at the apastron. The saturation value of orbital

eccentricity becomes $e = 0.57$. This value is estimated by equating the angular frequency at the inner edge of circumbinary disk with the orbital frequency at the apastron.

2.3. Gravitational-wave driven phase

The merging rate by the emission of gravitational wave can be written by(Peters 1964) as

$$\frac{\dot{a}(t)}{a(t)} = -\frac{256G^3M_{\rm bh}^3}{5c^5a^4}\frac{q}{(1+q)^2}\frac{f(e)}{(1-e^2)^{7/2}}, \tag{22}$$

where $f(e) = 1 + 73e^2/24 + 37e^4/96$. The coalescent timescale is then given as

$$t_{\rm gw} = \left|\frac{a(t)}{\dot{a}(t)}\right| = \frac{5}{32}\left(\frac{a(t)}{r_{\rm S}}\right)^4\frac{r_{\rm S}}{c}\frac{(1+q)^2}{q}(1-e^2)^{7/2}, \tag{23}$$

where $r_{\rm S} = 2GM_{\rm bh}/c^2$ is the Schwarzschild radius.

The semi-major axis decays to the transition radius, $a_{\rm t}$ where the emission of gravitational wave is more efficient than the binary-disk interaction. In other words, $t_{\rm gw}$ becomes shorter than $t_{\rm c}^{\rm gas}$ inside the transition radius. Comparing equation (20) with equation (23), the transition radius is defined by

$$\frac{a_{\rm t}}{r_{\rm S}} = \left[\frac{32}{5}\frac{ct_{\rm c}^{\rm gas}}{r_{\rm S}}\frac{q}{(1+q)^2}\frac{f(e)}{(1-e^2)^{7/2}}\right]^{1/4}. \tag{24}$$

When the timescale of orbital decay by the emission of gravitational radiation is shorter than the viscous timescale measured at the inner edge, the circumbinary disk is decoupled with the binary. The decoupling radius is then defined by

$$\frac{a_{\rm d}}{r_{\rm S}} = \left[\frac{32}{5}\frac{ct_{\rm vis,S}}{r_{\rm S}}\frac{q}{(1+q)^2}\frac{f(e)}{(1-e^2)^{7/2}}\right]^{4/11} \tag{25}$$

for the standard disk, and

$$\frac{a_{\rm d}}{r_{\rm S}} = \left[\frac{32}{5}\frac{ct_{\rm vis,S}}{r_{\rm S}}\frac{q}{(1+q)^2}\frac{f(e)}{(1-e^2)^{7/2}}\right]^{2/7} \tag{26}$$

for the self-regulated, self-gravitating disk. Here $t_{\rm vis,S}$ is the viscous timescale measured at the inner edge of circumbinary disk when $a(t) = r_{\rm S}$. Depending on the disk model, it can be written as

$$t_{\rm vis,S} \sim 5.9\times10^2[{\rm yr}]\left(\frac{0.1}{\alpha_{\rm SS}}\right)\left(\frac{0.1}{\eta}\right)^{1/4}\left(\frac{\epsilon}{0.1}\right)^{1/4}\left(\frac{\rm M_{bh}}{10^7{\rm M}_\odot}\right)^{5/4} \tag{27}$$

for the standard disk, and

$$t_{\rm vis,S} \sim 5.6\times10^4[{\rm yr}]\left(\frac{0.06}{\alpha_{\rm sg}}\right)^{1/3}\left(\frac{0.1}{\eta}\right)^{2/3}\left(\frac{\epsilon}{0.1}\right)^{2/3}\left(\frac{\rm M_{bh}}{10^7{\rm M}_\odot}\right)^{1/3} \tag{28}$$

for the self-regulated, self-gravitating disk, respectively.

Integrating equation (22), we obtain

$$\frac{a(t)}{a_{\rm t}} = \left(1 - \frac{t}{t_{\rm c}^{\rm gw}}\right)^{1/4}, \tag{29}$$

where $t_{\rm c}^{\rm gw}$ can approximately be written as

$$t_{\rm c}^{\rm gw} \simeq 3.8 \times 10^{11}[{\rm yr}] \left(\frac{a(t)}{a_{\rm t}}\right)^4 \left(\frac{M_{\rm bh}}{10^7 M_\odot}\right)^{-3} \frac{(1+q)^2}{q} \cdot \times (1-e_0^2)^{7/2}, \tag{30}$$

where $e_0 = 0.57$ is the initial orbital eccentricity at $a_{\rm t}$.

2.4. Observable period range for binary black holes

The resonant/tidal interaction causes the mass transfer from the circumbinary disk to accretion disk around each black hole(Hayasaki et al. 2007). The ram pressure by mass transfer acts on the outer edge of accretion disk and gives a one-armed oscillation on the disk (cf. Hayasaki & Okazaki 2005). The one-armed wave propagates from the outer edge to the black hole, which allows gas to accrete onto the black hole within the orbital period. This is repeated every binary orbit. This mechanism therefore originates periodic light variations synchronized with the orbital period(Hayasaki et al. 2008).

For the observational purpose, a_{10} is defined as the semi-major axis corresponding to feasible orbital period, 10yr, detectable with MAXI and/or Swift/BAT by

$$a_{10} \sim 4.9 \times 10^{-3}[{\rm pc}] \left(\frac{\rm M_{bh}}{10^7 \rm M_\odot}\right)^{1/3}. \tag{31}$$

Fig. 1 shows the mass dependence of each orbital period evaluated at $a_{\rm t}$, $a_{\rm d}$, and a_{10} for equal-mass binary massive black holes. The dashed line, dotted line and horizontal dash-dotted line show the orbital period at $a_{\rm t}$, $a_{\rm d}$, and a_{10}, respectively. The area filled in with the solid line shows the existential region of binary black hole candidates with periodic light-curve signatures detectable with MAXI and/or Swift/BAT.

Fig. 2 shows the mass dependence on each characteristic semi-major axis, $a_{\rm h}$, $a_{\rm t}$, $a_{\rm d}$, and a_{10}, for the equal-mass binary. All of the semi-major axes get longer as black hole mass is more massive. The decoupling radius is described by equation (25) when $M_{\rm bh} \lesssim 3 \times 10^6 M_\odot$, whereas it is described by equation (26) when $M_{\rm bh} \gtrsim 3 \times 10^6 M_\odot$. Note that a_{10} is on the track, where the binary evolves by the binary-disk interaction, when $M_{\rm bh} \lesssim 2 \times 10^7 M_\odot$, whereas a_{10} is on the track, where the binary evolves by the emission of gravitational wave, when $M_{\rm bh} \gtrsim 2 \times 10^7 M_\odot$.

Fig. 3 shows the orbital-decay timescale, $|a/\dot{a}|$, of binary massive black holes with $M_{\rm bh} = 10^{7.5} M_\odot$ in panel (a) and corresponding elapsed time in panel (b). The dashed line shows the timescale in the first evolutionary phase where the orbit decays by the dynamical friction (hereafter, dynamical-friction driven phase). The solid line shows the timescale in the second evolutionary phase where the orbit decays by the binary-disk interaction (hereafter, disk-driven phase). The dotted line shows the timescale in the final phase where the orbit decays by the dissipation due to the emission of the gravitational wave (hereafter, gravitational-wave

driven phase). The dash-dotted line shows the orbital-decay timescale of by stellar scattering (hereafter, stellar-scattering driven phase). We note that the orbital-decay timescale of stellar-scattering driven phase is too long for stellar scattering to be efficient mechanism in binary evolution. The binary therefore evolves toward coalescence via first dynamical-friction driven phase, second disk-driven phase, and final gravitational-wave driven phase. The orbital-decay timescale of disk-driven phase is the longest among the other two.

Fig. 4 shows the orbital-decay timescale of the binary with the same format as that of panel (a) of Fig. 3, but for $M_{\rm bh} = 10^6 M_\odot$. Note that stellar scattering is efficient after hardening of the binary, as shown in the dash-dotted line of Fig. 4.

3. Mass function of binary massive black holes

Observed black-hole mass function of nearby AGNs allows one to study mass functions of binary massive black holes based on the evolutionary scenario described in the previous section. Fig. 5 shows the fractional mass function of hard X-ray selected AGNs in the local universe, where the black hole mass is estimated from the K-band magnitudes of their host galaxies, as compiled by Winter et al. (2009). This mass function is 99% complete for the uniform sample of local Seyfert galaxies, and hence the uncertainties caused by the sample incompleteness should be regarded negligible.

Assuming that two galaxies start randomly to merge during the interval, t_*, where t_* is the look back time from present universe, a probability for finding binary massive black holes in the present universe can be expressed by $|a/\dot{a}|/t_*$. The number of binary massive black holes, $N_{\rm bbh}$, in AGNs can be obtained by $N_{\rm bbh} = f_{\rm c}(|a/\dot{a}|/t_*)/N_{\rm AGN}$, where $N_{\rm AGN}$ is the number of AGNs and $f_{\rm c}$ is a dimensionless fraction parameter. More than 25% of the host galaxies of Swift/BAT AGNs show evidence for on-going mergers (Koss et al. 2010), where the separation between central two cores in the merging galaxies is more than *kpc* scale. Therefore, we set $f_{\rm c} = 0.75$ unless otherwise noted, since we discuss binary black holes with a separation of much smaller scale.

One can estimate the probability for finding binary black holes in nearby AGNs by putting $t_{\rm AGN}$ into t_*, where $t_{\rm AGN} = M_{\rm bh}/\dot{M}_{\rm acc}$ shows the e-holding accretion timescale which corresponds to the typical lifetime of AGNs. Fig. 6 (a) and (b) show the mass-dependences of $|a/\dot{a}|/t_{\rm AGN}$, evaluated for $q = 1.0$ and $q = 0.1$, respectively. The dashed line, dash-dotted line and dotted line show the probability for finding binary black holes with $a_{\rm h}$, $a_{\rm t}$, and $a_{\rm d}$, respectively. It is noted from both panels that the probability of $a_{\rm h}$ is lower than that of $a_{\rm t}$ in the mass range less than the order of $10^6 M_\odot$, because the binary more rapidly evolves by stellar scattering than by disk-binary interaction as shown in the dash-dotted line of Fig. 4. The probability evaluated at $a_{\rm t}$ keeps constant over all of mass-ranges.

The solid line shows the integrated probability for finding binary black holes with the semi-major axis less than a_{10}. The integrated probability is approximately given by $\Delta t/t_{\rm AGN}$,

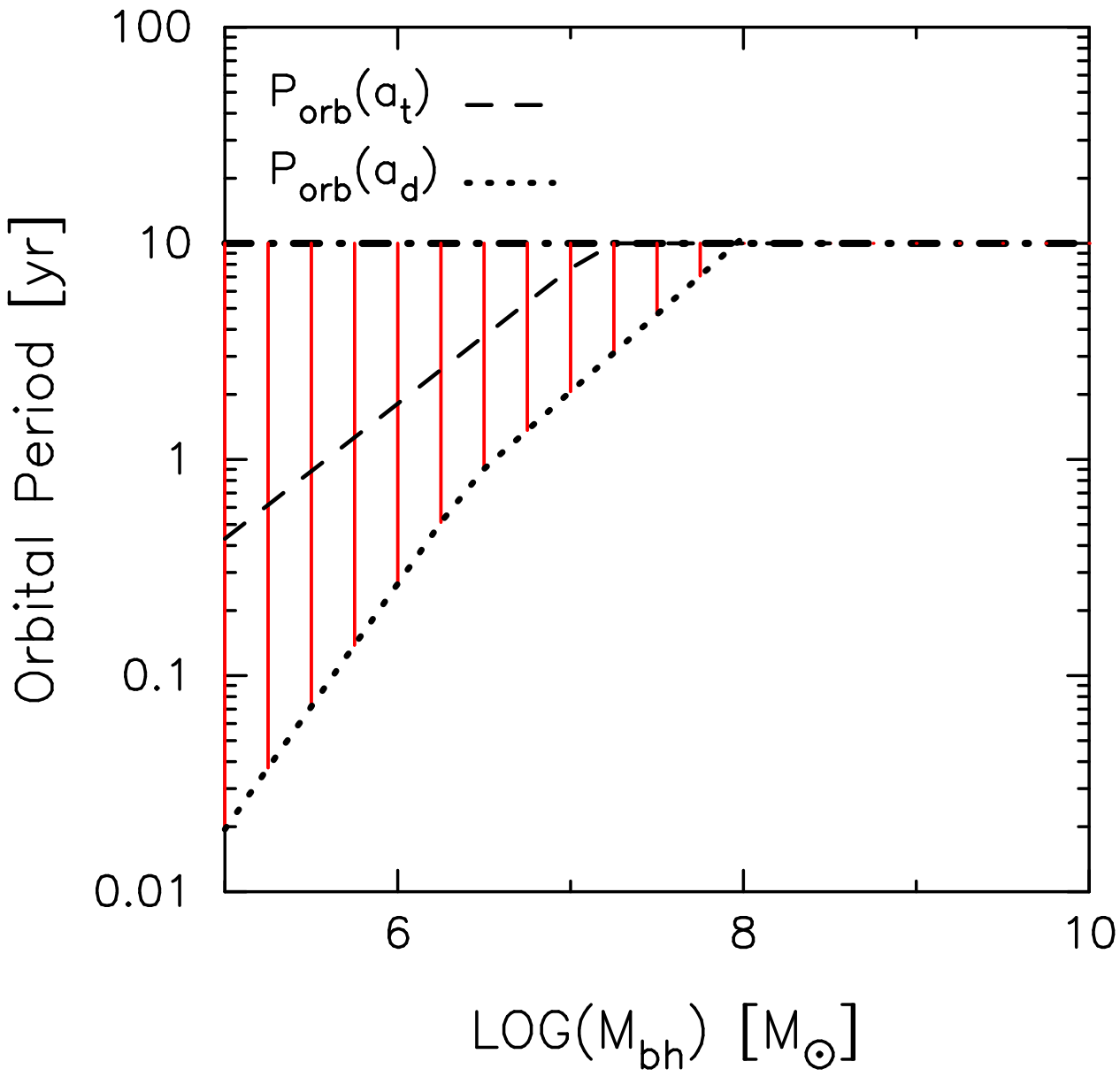

Fig. 1. Observable period range of binary massive black holes with characteristic semi-major axes. The dashed line shows the mass dependence of the orbital period evaluated at the transition radius, $a_{\rm t}$, where the dominant mechanism of binary evolution changes from the angular momentum loss by the binary-disk interaction to the dissipation by emitting gravitational wave radiation. The dotted line shows the one evaluated at the decoupling radius, $a_{\rm d}$, where the circumbinary disk decouples with binary massive black holes. The horizontal dash-dotted line shows the orbital period of ten years. The region drawn in solid lines shows the mass dependence of the orbital period less than ten years, which is detectable with MAXI and/or Swift.

where

$$\Delta t = \begin{cases} t_{\rm c}^{\rm gas} \ln\left(a_{10}/a_{\rm t}\right) + t_{\rm c}^{\rm gw}(a_t) - t_{\rm c}^{\rm gw}(a_{\rm d}) & a_{10} \geq a_{\rm t} \\ t_{\rm c}^{\rm gw}(a_{10}) - t_{\rm c}^{\rm gw}(a_{\rm d}) & a_{10} \leq a_{\rm t}, \end{cases} \tag{32}$$

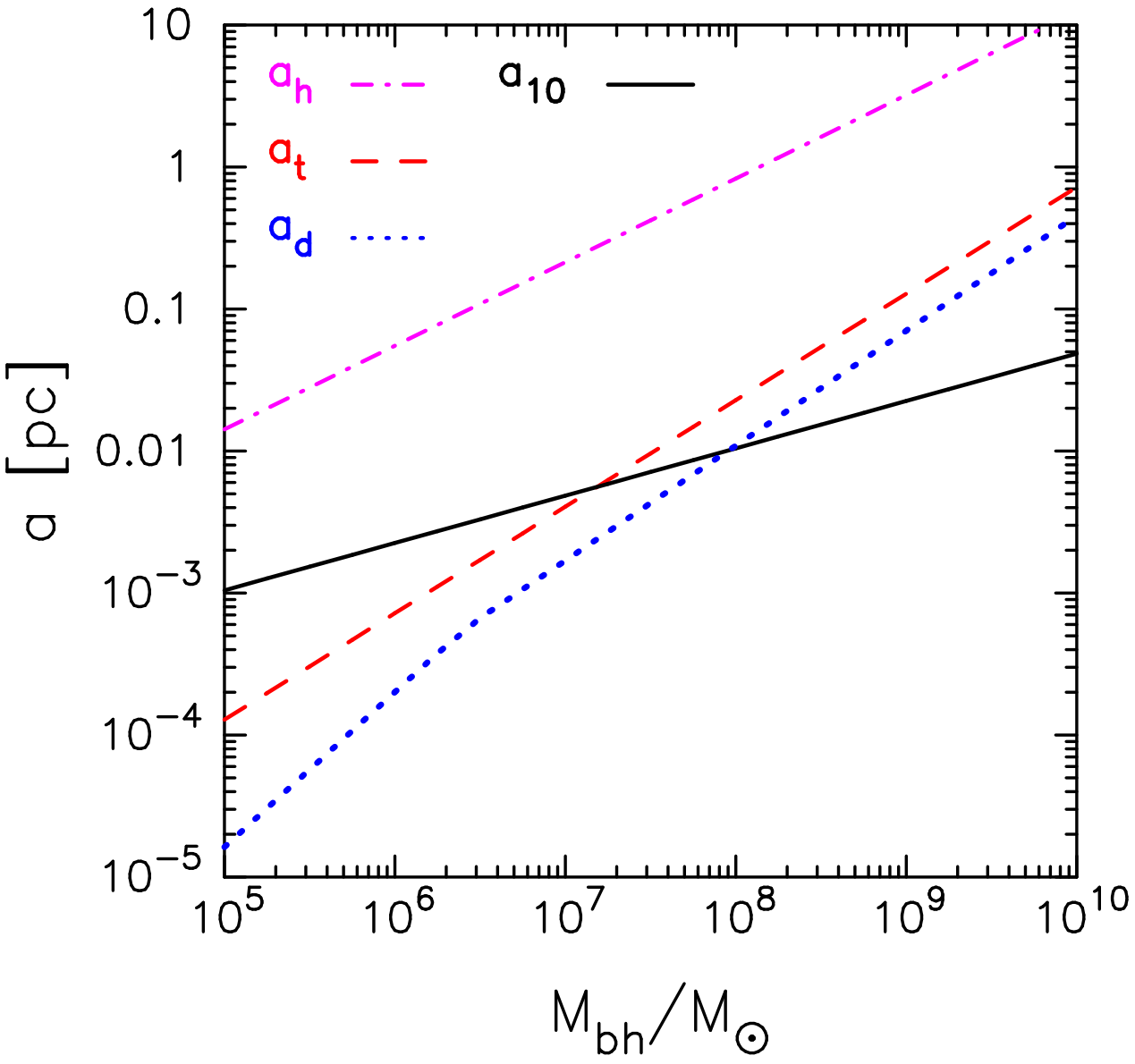

Fig. 2. Mass dependence of characteristic semi-major axes of binary massive black holes. The solid line shows the radius corresponding to the orbital period of ten years, a_{10}. The dashed line and dotted line show the transition radius, $a_{\rm t}$, and decoupling radius, $a_{\rm d}$, respectively. The dash-dotted line shows the hardening radius, $a_{\rm h}$, where the binding energy per unit mass of the binary equals to the kinetic energy of a star surrounding the binary.

from equation (20), (21), (29), and (30).

The integrated probability estimated for $a_{\rm d} \leq a \leq a_{10}$ is the monotonically decreasing function of black hole mass. Note that they rapidly decreases as the black hole mass becomes greater than $10^7 M_\odot$ for $q = 1.0$ and $5 \times 10^7 M_\odot$ for $q = 0.1$.

Fig. 7 shows mass functions of binary massive black holes in AGNs. The mass function is defined by multiplying the black-hole mass function of AGNs by the probability for finding binary black holes. The mass functions evaluated at the hardening radius, $a_{\rm h}$ and transition

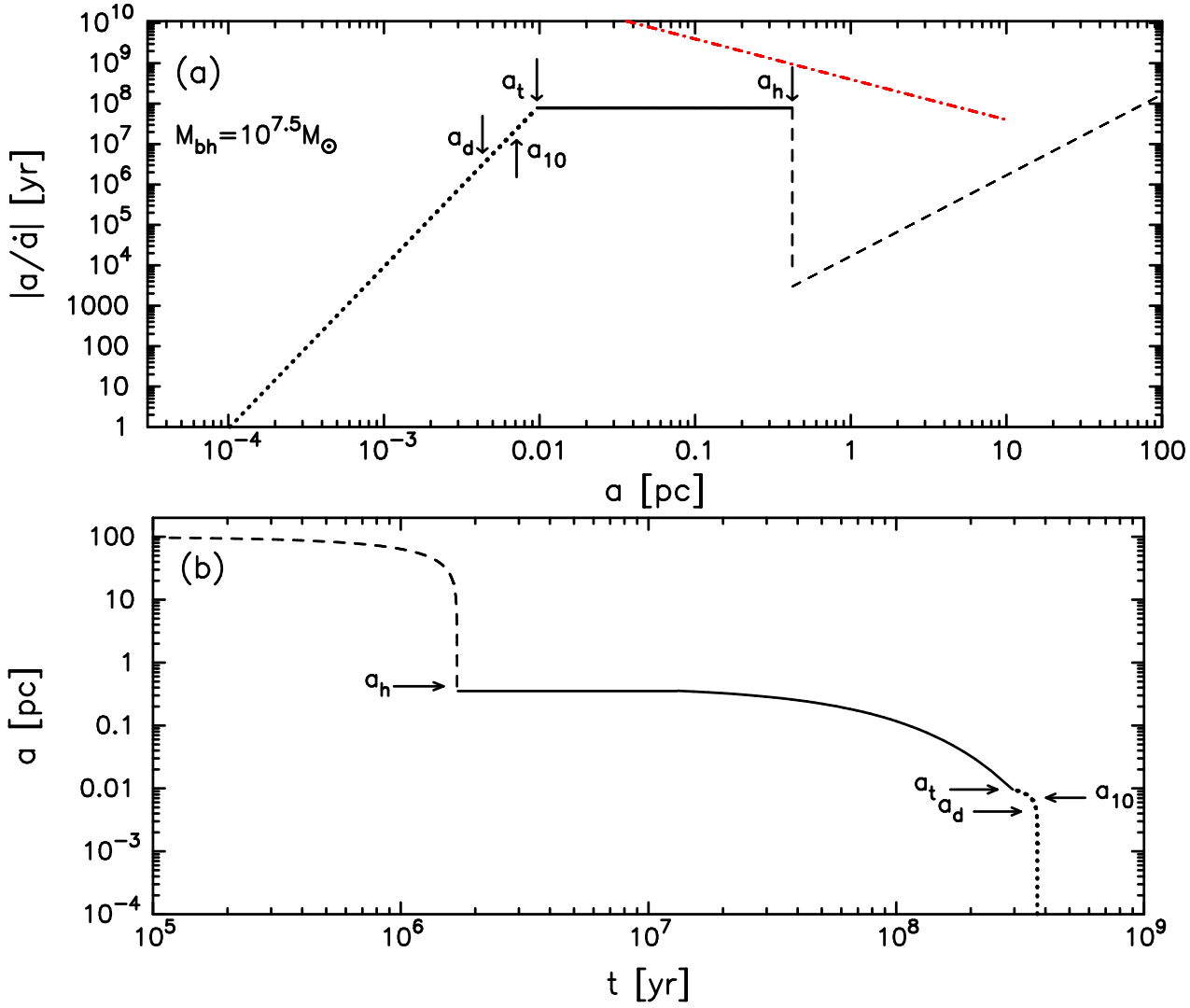

Fig. 3. (a) Orbital-decay timescale, $|a/\dot{a}|$, of evolution of binary massive black holes with a semi-major axis from 100pc to 10^{-4}pc. The total black hole mass is $M_{\rm bh} = 10^{7.5} M_\odot$ with equal mass ratio, $q = 1.0$. (b) Corresponding elapsed time of evolution of binary massive black holes. In both panels, the dashed line shows the first evolutionary phase in which two black holes get close each other toward the hardening radius, $a_{\rm h}$, by their angular momentum loss due to the dynamical friction with surrounding field stars. The solid line shows the second evolutionary phase from $a_{\rm h}$ to $a_{\rm t}$ in which the angular momentum of the binary is removed by binary-disk interaction. The binary evolves from $a_{\rm h}$ to $a_{\rm t}$ where the stage changes from the disk-driven phase to the gravitational-wave driven phase in which binary massive black holes finally coalesce by the emission of the gravitational radiation. There is the decoupling radius, $a_{\rm d}$, in the third evolutionary phase shown in the dotted line. In panel (a), the dash-dotted line shows the timescale of orbital decay by stellar scattering.

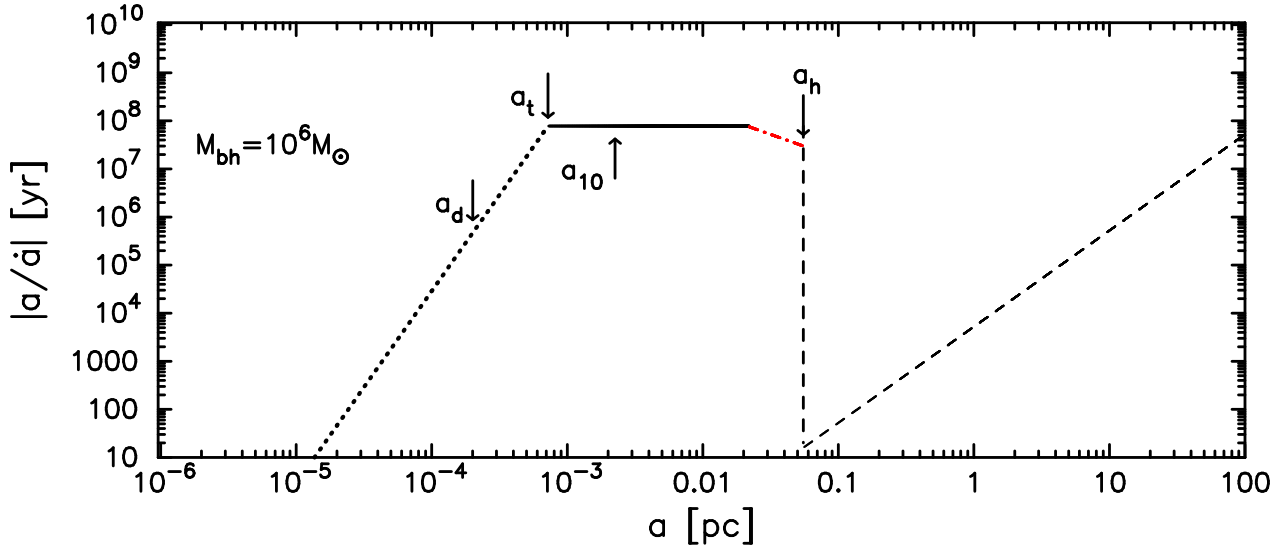

Fig. 4. Same format as panel (a) of Fig. 3, but for $M_{\rm bh} = 10^6 M_\odot$.

radius, $a_{\rm t}$, are exhibited in panel (a) and (b), respectively. In both panels, the solid line and the dashed line show the mass function with $q = 1.0$ and that with $q = 0.1$, respectively.

There is less population of binaries with mass less than $10^{6.5} M_\odot$ in panel (a), because the binary more rapidly evolves by stellar scattering than by disk-binary interaction in the mass range, as shown in the dash-dotted line of Fig. 4. Total fraction of binary black holes over all mass ranges are $(4.3 \pm 2\%)$ for $q = 0.1$ and $(13 \pm 4\%)$ for $q = 1.0$ in both panels (the quoted errors reflect the statistical uncertainties in the Swift/BAT AGN mass function). It is noted that from both panels that binary black holes of $M_{\rm bh} = 10^{8.5-9} M_\odot$ are the most frequent in the nearby AGN population.

Fig. 8 shows the mass functions of binary black holes with a constraint that the orbital period is less than ten years in both cases of $q = 1.0$ and $q = 0.1$. From the figure, binary black holes of $M_{\rm bh} = 10^{6.5-7} M_\odot$ for $q = 1.0$ and those of $M_{\rm bh} = 10^{7.5-8} M_\odot$ for $q = 0.1$ are the most frequent in the nearby AGN population. It is notable that, assuming that all the binaries have equal black-hole mass ratio, 18% of AGNs with black hole of $10^{6.5-7} M_\odot$ has binary black holes.

Total fraction of binary black holes over all mass ranges are $(1.8 \pm 0.6\%)$ for $q = 1.0$ and $(1.6 \pm 0.4\%)$ for $q = 0.1$. We can therefore observe $15 \sim 27$ candidates for 1300 AGNs detectable with MAXI, assuming that activities of all nearby AGNs lasts for $t_{\rm AGN} = M_{\rm bh}/\dot{M}_{\rm acc}$. Note that MAXI covers the softer energy band (2–30 keV) than Swift/BAT (15–200 keV), and hence the ratio of type-1 (unabsorbed) AGNs to type-2 (absorbed) AGNs will be higher in the MAXI survey (≈8:5 based on the model by Ueda et al. 2003) than in the Swift/BAT survey (≈1:1, Tueller et al. 2010). Here we have referred to the same AGN mass function, however, since we do not find statistically significant difference between the observed mass functions of type-1 and type-2 AGNs based on the Kolmogorov-Smirnov test.

4. Summary & Discussion

We study mass functions of binary massive black holes on the subparsec scale in AGNs based on the evolutionary scenario of binary massive black holes with surrounding gaseous disks in the framework of coevolution of massive black holes and their host galaxies.

As a very recent progress in observations of binary massive black holes with the Sloan Digital Sky Survey (SDSS), there is a claim that two broad emission line quasars with multiple redshift systems are subparsec binary candidates(Borson & Lauer 2009). The temporal variations of such the emission lines are attributed to the binary orbital motion(Loeb 2009; Shen & Loeb 2009). These can be used as complementary approaches to search for binary massive black holes with MAXI and/or Swift/BAT.

Recently, Volonteri et al. (2009) predicted the fraction of binary quasars at $z < 1$ based on the theoretical scenario for the hierarchical assembly of supermassive black holes in a ΛCDM cosmology. They adopted the merging timescale of binary black holes with a circumbinary disk estimated by Haiman et al. (2009), in order to explain the observed paucity of binary quasars in the SDSS sample (2 out of 10000; Bogdanović et al. 2009; Dotti et al. 2009; Borson & Lauer 2009). For the black hole mass range of $\sim 10^8 M_\odot$, which these SDSS quasars likely have, our calculation gives a similar merging timescale ($\sim 10^8$ year, independent of mass). Hence, our model will also be compatible with the SDSS results when applied to the same cosmological model. In a lower mass range, however, we predict a significantly longer merging timescale, by a factor of 10 at $\sim 10^7 M_\odot$, than that by Haiman et al. (2009), which rapidly decreases with the decreasing mass. Hence, much larger fractions of subparsec binary black holes are expected in our model than in Volonteri et al. (2009) if low mass black-holes are considered.

Kocsis & Sesana (2010) studied the nHz gravitational wave background generated by close binary massive black holes with orbital periods between 0.1-10 years, taking account of both the cosmological merger rate and such the binary-disk interaction as the planetary (type II) migration(Haiman et al. 2009). The orbital-decay timescale for low black-hole mass binaries ($M_{\rm bh} \leq 10^7 M_\odot$) is much shorter than that of our model. This suggests that little stochastic gravitational wave background is attenuated by applying our model for their scenario, because the amplitude of gravitational wave background is proportional to the root of ratio of the orbital-decay timescale of the disk-driven phase to that of the gravitational-wave driven phase.

Our main conclusions are summarized as follows:

(1). Binary massive black holes on the subparsec scale can merge within a Hubble time by the interaction with triple disk consisting of an accretion disk around each black hole and a circumbinary disk surrounding them. Assuming that the circumbinary disk is steady, axisymmetric, geometrically thin, self-regulated, self-gravitating but non-fragmenting with a fraction of Eddington accretion rate, its orbital-decay timescale is given by $\sim 3.1 \times 10^8 q/(1+q)(0.1/\eta)(\epsilon/0.1)$[yr], where q, η, and ϵ show the black-hole mass ratio, Eddington

ratio, and mass-to-energy conversion efficiency, respectively.

(2). Binary black holes of $M_{\rm bh} = 10^{8.5-9} M_\odot$ in the disk-driven phase are the most frequent among the AGN population. Assuming that activities of all nearby AGNs lasts for the accretion timescale, $M_{\rm bh}/\dot{M}_{\rm acc}$, the total fraction of binaries with the semi-major axis evaluated at the hardening radius and transition radius are estimated as $(4.3 \pm 2\%)$ and $(13 \pm 4\%)$, respectively.

(3). Assuming that all binary massive black holes have the equal mass ratio ($q = 1.0$), $\sim 20\%$ of AGNs with $M_{\rm bh} = 10^{6.5-7} M_\odot$ harbor binary black holes with orbital period less than ten years in their center. This black-hole mass range therefore provides the best chance to find such close binary black holes in AGNs.

(4). The total fraction of close binary massive black holes with orbital period less than ten years, as is detectable with MAXI and/or Swift/BAT, can be estimated as $(1.8 \pm 0.6\%)$ for $q = 1.0$ and $(1.6 \pm 0.4\%)$ for $q = 0.1$.

We thank anonymous referee for the useful comments and suggestions. We also thank Mike Koss and Richard Mushotzky for providing us with the latest result on the merging rate of Swift/BAT AGNs before publication. KH is grateful to Atsuo T. Okazaki, Takahiro Tanaka, and Stanley P. Owocki for helpful discussions. This work has been supported in part by the Ministry of Education, Science, Culture, and Sport and Technology (MEXT) through Grant-in-Aid for Scientific Research (19740100, 18104003, 21540304, 22340045, 22540243 KH and 20540230 YU, and 22740120 IN), and by the Grant-in-Aid for the Global COE Program "The Next Generation of Physics, Spun from Universality and Emergence" from MEXT of Japan.

References

Armitage, P. J., & Natarajan, P. 2002, ApJ, 567, L9
Armitage, P. J., & Natarajan, P. 2005, ApJ, 634, 921
Artymowicz, P., & Lubow, S. H. 1994, ApJ, 421, 651
Begelman, M. C., Blandford, R. D., & Rees, M. J. 1980, Nature, 287, 307
Berentzen, I., Preto, M., Berczik, P., Merritt, D., & Spurzem, R, 2009, ApJ, 695, 455
Binney, J., & Tremaine, S. 1987, Galactic Dynamics (Princeton: Princeton University Press), 428
Bertin,G. 1997, ApJ, 478, L71
Bogdanović, T., Smith, B. D., Sigurdsson, S., & Eracleous, M. 2008, ApJ, 174, 455
Bogdanović, T., Eracleous, M., & Sigurdsson, S. 2009, ApJ, 697, 288
Borson, T. A., & Lauer, T. R. 2009, Nature, 458, 53
Cuadra, J., Armitage, P. J., Alexander, R. D., & Begelman, M. C. 2009, MNRAS, 393, 1423
Di Matteo, T., Springel, V., & Hernquist, L. 2005, Nature, 433, 604
Dotti, M., Colpi, M., Haardt, F., & Mayer, L. 2007, MNRAS, 379, 956
Dotti, M., Montuori, C., Decarli, R., Volonteri, M., Colpi, M., & Haardt, F. 2009, MNRAS, 398, 73

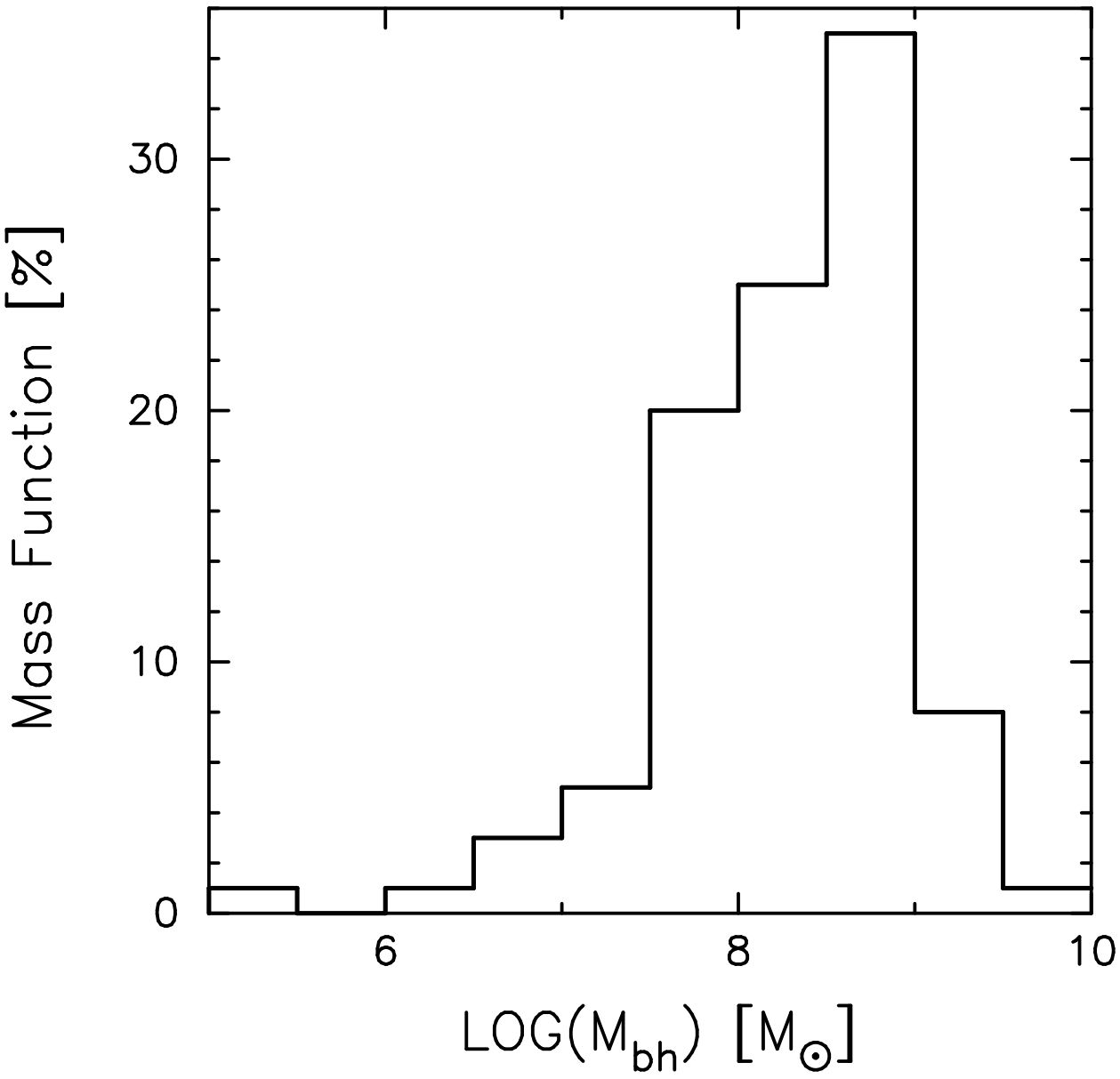

Fig. 5. Normalized mass function of massive black holes in AGNs, detected with Swift/BAT (15–200 keV) given by Winter et al. (2009).

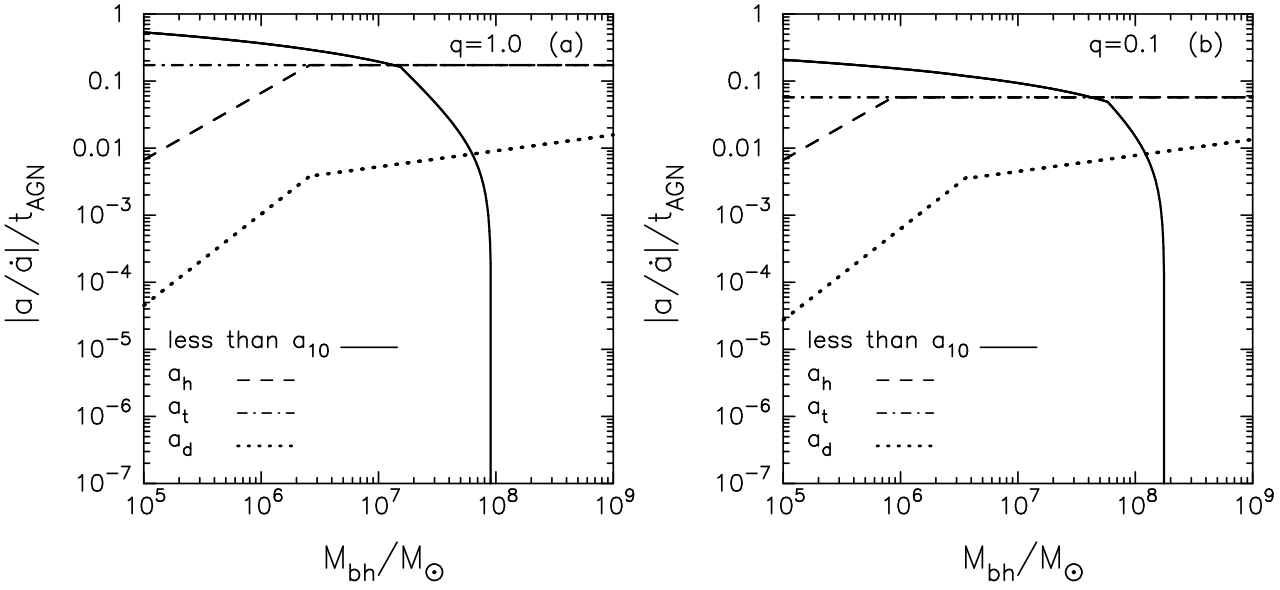

Fig. 6. Mass dependence of probabilities for finding binary massive black holes evaluated for q=1.0 (a) and q=0.1 (b). The probability is defined as the orbital-decay timescale normalized by the accretion timescale, $|a/\dot{a}|/t_{\rm AGN}$, where $t_{\rm AGN} = M_{\rm bh}/\dot{M}_{\rm acc}$. The solid line shows the integrated probability for finding binary massive black holes with the semi-major axis from a_{10} to $a_{\rm d}$. The dashed line, dash-dotted line, and dotted line show the probabilities evaluated at $a_{\rm h}$, $a_{\rm t}$, and $a_{\rm d}$, respectively.

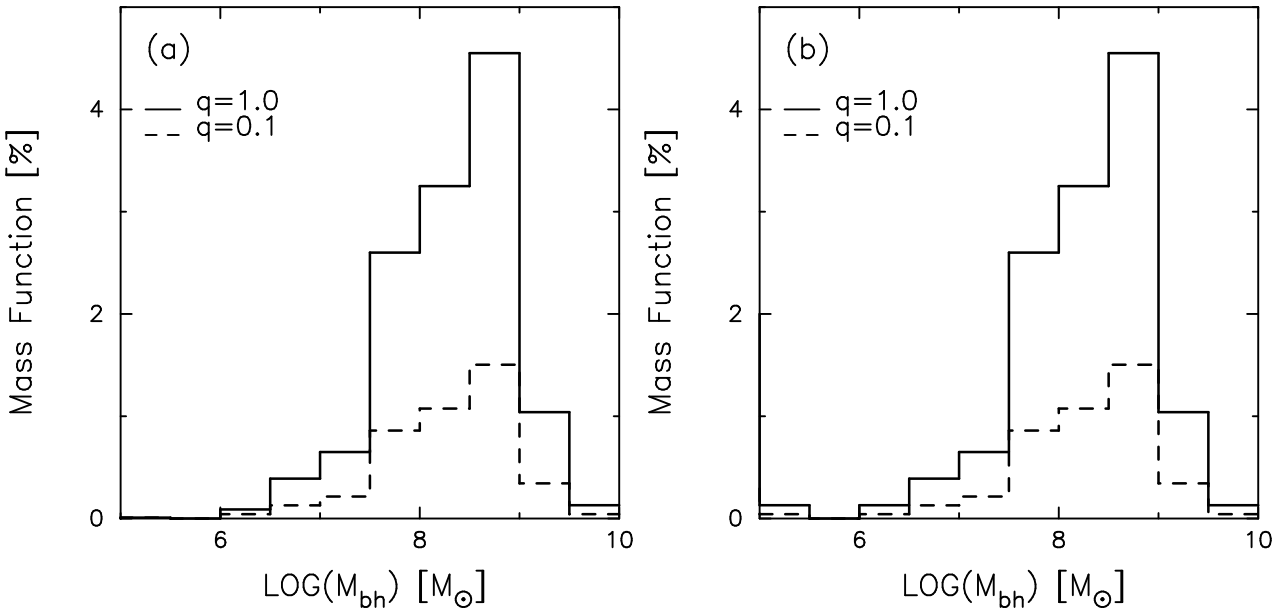

Fig. 7. Mass functions of binary massive black holes in AGNs evaluated at the hardening radius, $a_{\rm h}$, (a) and transition radius, $a_{\rm t}$, (b). They are defined by multiplying the mass function of AGNs by the probability for finding binary massive black holes.

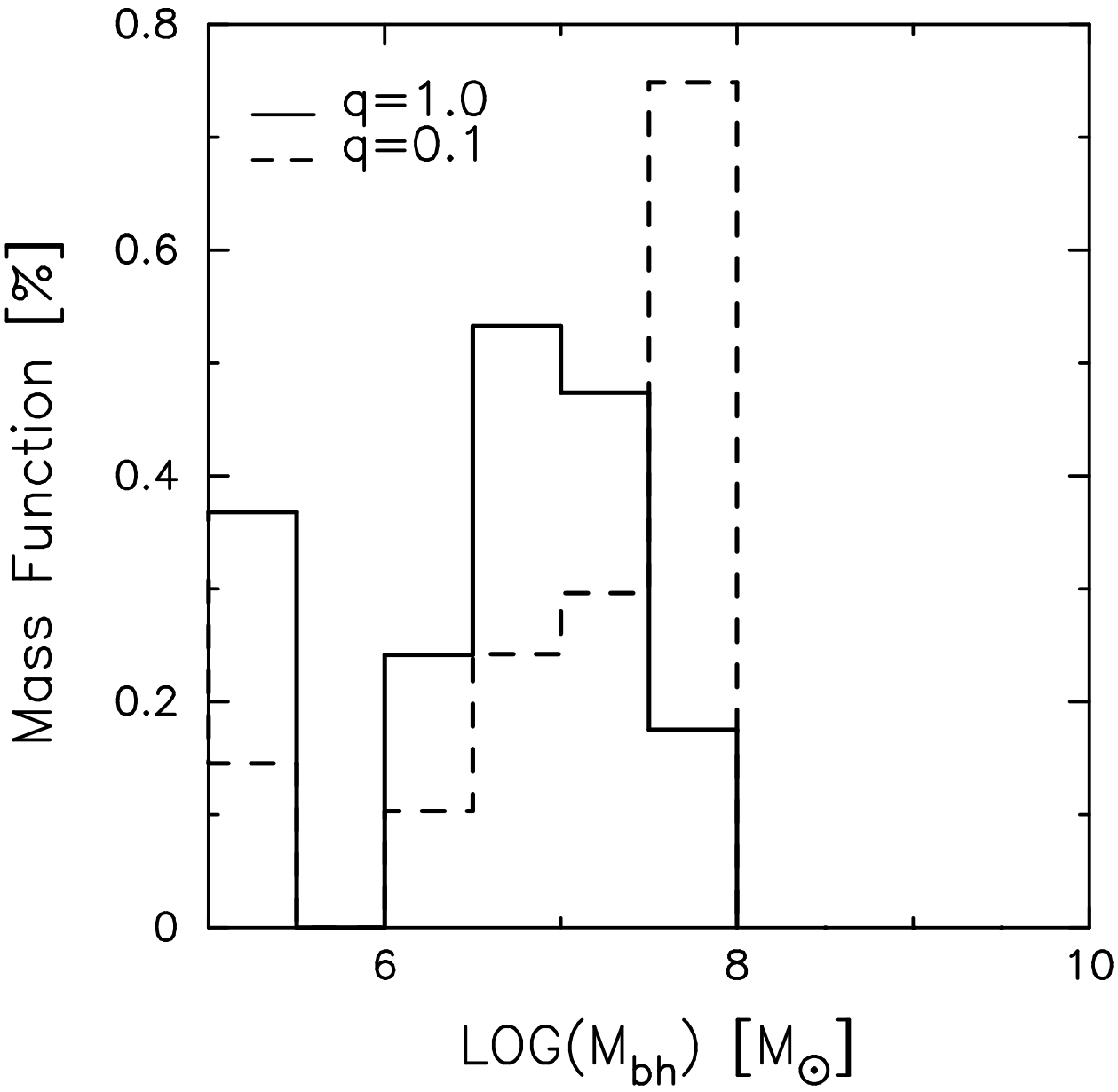

Fig. 8. Mass functions of close binary massive black holes with the orbital period less than ten years. Same formats as Fig. 7.

Ebisuzaki, T., Makino, J., & Okamura, S. K. 1991, Nature, 354, 212
Escala, A., Larson, R. B., Coppi, P. S., & Mardones, D. 2005, ApJ, 630,152
Ferrarese, L., & Merritt, D. 2000, ApJ, 539. L9
Gould, A., & Rix, H. 2000, ApJ, 532, L29
Gebhardt, K., et al. 2000, ApJ, 539, L13
Haiman, Z., Kocsis, B., & Menou, K. 2009, ApJ, 700, 1952
Hayasaki, K., Mineshige, S., & Ho, C. L. 2008, ApJ, 682, 1134
Hayasaki, K., Mineshige, S., & Sudou, H. 2007, PASJ, 59, 427
Hayasaki, K. 2009, PASJ, 61, 427
Hayasaki, K., & Okazaki, A.T. 2005, MNRAS, 360, L15
Ivanov, P. B., Papaloizou, J. C. B., & Polnarev, A. G. 1999, MNRAS, 307, 79
Iwasawa, M., Funato, Y., & Makino, J. 2006, ApJ, 651, 1059
Kocsis, B., & Sesana, A. 2010, arXive1002.0584
Komossa, S., Burwitz, V., Hasinger, G., Predehl, P., Kaastra, J. S., & Ikebe, Y. 2003, ApJ, 582, L15
Kormendy, J., & Richstone, D. 1995, ARA&A, 33, 581
Kormendy, J., & Bender, R. 2009, ApJ, 691, L142
Koss, M., Mushotzky, R., Veilleux, S., & Winter, L. M. 2010, ApJ, 716, L125
Lodato, G., Nayakshin, S., King, A. R., & Pringle, J. E. 2009, 398, 1392
Loeb, A. 2010, PhRvD, 81, 047503
MacFadyen, I. A., & Milosavljević, M. 2008, ApJ, 672, 83
Magorrian, J., et al. 1998, AJ, 115, 2285
Makino, J. 1997, ApJ, 478, 58
Matsubayashi, T., Makino, J., & Ebisuzaki, T. 2007, ApJ, 656, 879
Matsui, M., & Habe, A. 2009, PASJ, 61, 421
Matsuoka, M., et al. 2009, PASJ, 61,999
Mayer, L., Kazantzidis, S., Madau, P., Colpi, M., Quinn, T., & Wadsley, J. 2007, Science, 316, 1874
Merritt, D., & Milosavljević, M. 2005, Living Rev. Relativity, 8, 8
Milosavljević, M., & Merritt, D. 2001, ApJ, 563, 34
Milosavljević, M., & Merritt, D. 2003, ApJ, 596, 860
Mineshige, S., & Umemura, M. 1996, ApJ, 469, L49
Peters, P. C. 1964, Physical Review, 136, 1224
Quinlan, G. D. 1996, New Astron, 1, 35
Quinlan, G. D., & Hernquist, L. 1997, New Astron, 2, 533
Rice, W.K., Lodato, G., & Armitage, P. J. 2005, MNRAS, 364, L56
Shakura, N. I. & Sunyaev, R. A. 1973, A&A, 24, 337
Sesana, A., Haardt, F., & Madau, P. 2007, ApJ, 660, 546
Shen, Y., & Loeb, A. 2009, arXiv:0912.0541
Tueller, J., et al. 2010, ApJS, 186, 378
Ueda, U., Akiyama, M., Ohta, K., & Takamitsu, T. 2003, ApJ, 598, 886
Volonteri, M., Miller, J. M., & Dotti, M. 2009, ApJ, 703, L86
Winter, L. M., Mushotzky, R. F., Reynolds, C. S., & Tueller, J. 2009, ApJ, 690, 1322

Yu, Q., & Tremaine, S. 2002, MNRAS, 335, 965